Structural Differences in the Two Agonist Binding Sites of the *Torpedo* Nicotinic Acetylcholine Receptor Revealed by Time-Resolved Fluorescence Spectroscopy[†]

K. L. Martinez,[‡] P. J. Corringer,[§] S. J. Edelstein,[||] J. P. Changeux,[§] and F. Mérola*,[‡]

Laboratoire pour l'Utilisation du Rayonnement Electromagnétique, Centre Universitaire Paris-Sud, B.P. 34, 91898 Orsay Cedex, France, Unité de Neurobiologie Moléculaire, Institut Pasteur, 75734 Paris, France, and Département de Biochimie, Université de Genève, CH-1211 Genève 4, Switzerland

Received December 8, 1999; Revised Manuscript Received March 23, 2000

ABSTRACT: The nicotinic acetylcholine receptor (nAChR) from *Torpedo marmorata* carries two nonequivalent agonist binding sites at the $\alpha\delta$ and $\alpha\gamma$ subunit interfaces. These sites have been characterized by time-resolved fluorescence with the partial nicotinic agonist dansyl-C_6-choline (Dnscho). When bound to the detergent-solubilized receptor, the fluorescence lifetime distribution of Dnscho displays a characteristic signature, with four separable components at 0.2, 1.8, 7.2, and 18.3 ns, respectively. Competition experiments with the antagonist d-tubocurarine (dTC), known to bind preferentially to the $\alpha\gamma$ site, result in substantial changes of this signature, associated with a strong decrease in average fluorescence lifetime. Comparisons with two other competitive antagonists, α-conotoxin M1 and α-bungarotoxin, demonstrate that Dnscho binds with a similar affinity to the two sites but that the microenvironment of the probe is different for each site. Using a two-site binding model together with published equilibrium constants to describe the competitive binding of dTC and Dnscho, we reach a satisfactory description of the changes in fluorescence lifetimes and propose characteristic fluorescence parameters of the probe bound to each type of site. This analysis indicates that Dnscho at the $\alpha\delta$ site is principally associated with a 8.7 ns lifetime, while it has a 20.2 ns major lifetime at the $\alpha\gamma$ site. Therefore, the observed fluorescence heterogeneity arises in large part from the structural differences of the two binding sites. As a result, this signal can be used to identify the binding preferences of competitive ligands of unknown pharmacology.

At the neuromuscular junction, the acetylcholine (ACh)[1] released by the motor nerve ending binds to the postsynaptic nicotinic acetylcholine receptor (nAChR), resulting in membrane depolarization and muscle contraction. Homologous nAChR are highly abundant in the *Torpedo* electric organ, which facilitated their isolation, purification, and characterization. The protein is a heteropentamer composed of four homologous subunits, with the stoichiometry $\alpha_2\beta\gamma\delta$, possessing two binding sites per pentamer coupled to an axial cationic ion channel *(1)*. Upon binding to muscle-type nAChRs, ACh triggers a cascade of allosteric transitions, leading to rapid activation on the millisecond time scale, followed by slower relaxations to two desensitized states, an intermediate state in the millisecond to second time scale displaying high ACh affinity (I), and a desensitized state on the second to minute time scale displaying very high ACh affinity (D) *(2)*.

Strong evidence supports the notion that the two binding sites are respectively located at the $\alpha\gamma$ and $\alpha\delta$ subunit interfaces. The evidence include pairwise expression of the α/γ or α/δ subunits, which are sufficient to form ACh binding sites *(3)*, and affinity labeling experiments with a series of agonists and competitive antagonists that revealed the labeling of the α, γ, and δ subunits *(4−9)*. The identification of the labeled amino acids further showed that each subunit contributes three loops to the binding site, with the α subunit contributing loops A, B, and C (principal component), and the γ or δ subunits contributing loops D, E, and F (complementary component) *(10)*. Site-directed mutagenesis confirmed the intersubunit location of the Ach binding site in neuronal homomeric nAChR *(11−13)*.

Certain competitive antagonists, in particular d-tubocurarine (dTC) and α-conotoxin M1 (α-Ctx), display markedly different binding affinities for the two sites, a feature attributed to several nonconserved residues carried by the γ and δ subunit *(14, 15)*. Indeed, the equilibrium binding of the competitive antagonist [^{3}H]dTC is characterized, for the *Torpedo marmorata* receptor, by an apparent Hill coefficient close to 0.5, interpreted as reflecting two different binding affinities: 33 nM and 7.7 μM *(16)*. This interpretation was confirmed by affinity labeling of *T. marmorata* nAChR showing that DDF labeling was protected by dTC in a biphasic manner for the α subunit, whereas monophasic protection was observed for the γ and δ subunits (*17*; see also ref *8* for the *Torpedo californica* nAChR). These results also established that the dTC high-affinity binding

[†] K.L.M. was supported by a doctoral grant (96653) from the MENESR.

* Correspondence should be addressed to this author: e-mail fab@lure.u-psud.fr.

[‡] Centre Universitaire Paris-Sud.

[§] Institute Pasteur.

[||] Université de Genève.

[1] Abbreviations: nAChR, nicotinic acetylcholine receptor; ACh, acetylcholine; cmc, critical micellar concentration; α-Ctx, α-conotoxin M1; dTC, d-tubocurarine; α-Bgt, α-bungarotoxin; Dnscho, dansyl-C_6-choline; CHAPS, 3-[(3-cholamidopropyl)dimethylammonio]-1-propanesulfonate; DDF, *p*-(*N*,*N*-dimethylamino)benzenediazonium fluoroborate; FRET, fluorescence resonant energy transfer; NMR, nuclear magnetic resonance; fwhm, full width at half-maximum.

10.1021/bi992811p CCC: $19.00
Published on Web 05/16/2000

site is located at the $\alpha\gamma$ interface, with dissociation constants similar to those determined by direct binding. For α-Ctx, inhibition by [^{125}I]α-Bgt and competition with dTC suggest that, in the case of *T. californica* nAChR, this competitive antagonist also displays two distinct affinities for the agonist binding sites *(18)*. As in the case of dTC, the high-affinity site receptor was shown to lie at the $\alpha\gamma$ subunit interface *(18, 19)*, with affinity constants of 2.6 nM and 2.3 μM *(20)*, respectively, for the $\alpha\gamma$ and $\alpha\delta$ binding sites. However, the high-affinity site appears to be species-dependent, since the $\alpha\delta$ site possesses the higher affinity in the case of mouse fetal muscle receptor *(18)*. In contrast, α-Bgt was reported to interact with a homogeneous class of binding sites on the *T. marmorata* receptor membrane (K_d = 20 pM) *(16, 21)*.

Concerning the natural agonist ACh, differences in the affinity of the two sites has been reported in some cases but not in others. For example, no evidence was found for two nonidentical binding sites at equilibrium *(16)*. On the other hand, different binding affinities of activation for agonists were inferred from single-channel recordings on mouse and human muscle fibers [see references in Edelstein et al. *(22, 23)*]. The structural differences between the two sites may have important physiological consequences *(24)*.

The nAChR has been extensively studied by fluorescence techniques. Fluorescence resonant energy transfer (FRET) has been used for structural mapping of the protein *(25−28)*, while most ligand binding kinetics by rapid mixing techniques were performed with the fluorescent agonists NBD-5-acetylcholine *(29)* or dansyl-C_6-choline (Dnscho) *(2)*. Dnscho is a fluorescent partial agonist that was synthesized to follow the interactions of the nicotinic agonist with the nAChR *(30)* by use of FRET from tryptophan residues to the dansyl chromophore. The length of the aliphatic chain separating the choline and the dansyl group has been optimized to preserve unperturbed interactions of the choline moiety with the agonist binding sites. Below 100 μM, the probe binds specifically to the agonist binding sites *(2, 27)*. The binding affinities of this probe for the different allosteric states were estimated by Heidmann and Changeux (*2*) using stopped-flow and ion flux experiments as 20 nM and 60 μM for the desensitized (D) and basal (B) states, respectively, and in the micromolar range for the intermediate (I) and activated (A) states.

Time-resolved fluorescence is particulary sensitive to details of the local environment of a fluorescent chromophore and, when used at high resolution, can provide quantitative information about possible local microheterogeneity. Therefore, the technique is well suited to explore the chemical and physical events associated with ligand binding to membrane receptors. In this report, we present an analysis of the time-resolved fluorescence properties of Dnscho when bound to CHAPS-solubilized nAChR. We find that receptor-bound Dnscho displays a multiexponential fluorescence decay, and we use various competitive ligands to explore the molecular origins of this fluorescence heterogeneity. We further show that Dnscho has a very different fluorescence signal when bound to each of the two, nonequivalent binding sites of the receptor, with its two major fluorescence lifetimes each being associated with one type of binding site. Our results fit adequately with the current knowledge on the pharmacology of dTC and can be quantitatively interpreted in terms of the differential binding of this competitive ligand. Time-resolved fluorescence of Dnscho is thus the first spectroscopic signal to discriminate between the two agonist binding sites of muscle-type nicotinic receptors. These findings provide the basis for a new method for assessing preferential binding of new ligands.

MATERIALS AND METHODS

Materials. Torpedo marmorata electric fish were obtained from Arcachon or Roscoff, France. CHAPS, dTC, α-Ctx, proadifen, and dansylamide from Sigma and α-Bgt from Molecular Probes were used without further purification. Dnscho *(30)* was a generous gift from Professor B. Roques. Its purity was checked by NMR. The CHAPS buffer is composed of 5 mM Na_2PO_4, 1 mM EDTA, 100 mM NaCl, pH 7.2, and CHAPS, 6.5 mM final concentration. It was filtered and conserved by addition of NaN_3 (0.03% w/v).

nAChR Purification. The nAChR-rich membranes were prepared as described by Saitoh and Changeux *(31)* and then treated at pH 11 as described by Sobel et al. *(32)*. Alkaline-treated membranes were solubilized by the addition of CHAPS buffer. This procedure led to nearly homogeneous nAChR preparations in terms of protein content, as evaluated by SDS−PAGE. The protein concentration of the solubilized receptor was measured according to the Bradford method. Agonist binding site concentrations were then determined by steady-state fluorescence titration as described below. The specific activity for several sample preparations was in the range of 6 ± 1.4 nmol of agonist binding sites/mg of total protein, i.e., at least 70% of the total proteins have fully effective agonist binding sites, assuming two binding sites per receptor molecule of 300 000 Da. The nAChR functionality, in terms of capability to undergo allosteric transitions, was verified by stopped-flow experiments, according to Heidmann and Changeux *(2)* (manuscript in preparation).

Dnscho Binding Site Titration. The concentration of agonist binding sites was determined by steady-state fluorescence on a Spex spectrofluorometer, by use of FRET from the tryptophan residues of the receptor to bound Dnscho. Increasing volumes of solubilized nAChR solution were added to a Dnscho solution of known concentration (typically 500 μL at 0.5 μM) in a 0.2 × 1 cm cuvette thermostated at 20 °C. After a 3-min incubation, the emission at 550 nm ($\Delta\lambda$ = 13 nm) was recorded with an excitation at 280 nm ($\Delta\lambda$ = 1 nm). The concentration of agonist binding sites was then determined at the intercept between the asymptote and the slope at null ordinate of the titration curve.

Fluorescence Quantum Yield Estimation. The emission spectra were recorded with an excitation wavelength of 330 nm ($\Delta\lambda$ = 2 nm). Background intensities of buffer solutions were subtracted from all spectra. A photodiode signal was used to correct for fluctuations in the excitation light. These technical emission spectra ($\Delta\lambda$ = 2 nm) were used to estimate the approximate fluorescence quantum yields (Φ_f) of Dnscho in several buffers:

$$\Phi_{f_{\text{Dnscho/buffer}}} = \frac{I_{\text{Dnscho/buffer}}}{I_{\text{Dns/EtOH}}} \frac{A_{\text{Dns/EtOH}}}{A_{\text{Dnscho/buffer}}} \Phi_{f_{\text{Dnscho/EtOH}}} \quad (1)$$

where I is the intensity integrated over the wavelength

region 400−700 nm and *A* is the absorbance at 330 nm. The quantum yield of dansylamide in ethanol (0.39) was used as a reference *(33)*.

nAChR Sample Preparation for Fluorescence Studies. In all fluorescence studies with Dnscho, aliquots of solubilized nAChR (typically 5 μM agonist binding sites) were incubated 10 min with Dnscho prior to the fluorescence measurements. In competition experiments, the nAChR samples were preincubated overnight at 4 °C, with ligands at various concentration ratios. R_{ligand}, defined as the ratio of ligand concentration to the total concentration of agonist binding sites, was fixed between 0.1 and 0.7. The fluorescent probe was then added to each sample before fluorescence measurements in order to saturate 80% of the remaining free agonist binding sites, i.e., $R_{Dnscho} = 0.8(1 - R_{ligand})$, with R_{Dnscho} defined as the ratio of the total concentration of Dnscho to the total concentration of agonist binding sites.

Time-Resolved Fluorescence Measurements. Time-resolved fluorescence measurements were performed by the time-correlated single photon counting method *(34, 35)*, using synchrotron radiation as the source of the excitation light, as described in Deville-Bonne et al. *(36)*. The width of the excitation pulse collected on the SA1 beam line of Super-ACO (LURE) was routinely 650 ps fwhm, with a repetition frequency of 8.323 MHz. The excitation was set at 330 nm ($\Delta\lambda = 9$ nm) and the emission was observed at 520 nm ($\Delta\lambda = 9$ nm) for polarized experiments and at 520 nm ($\Delta\lambda = 36$ nm) for unpolarized experiments. All experiments were performed at 20 °C, with each curve collected over 2048 channels at 49 ps/channel, and 5−10 million counts stored in the total decay.

Analysis of the Time-Resolved Fluorescence Measurements. The fluorescence decays were analyzed by the maximum entropy method (FAME, MEDC Ltd., U.K.) as described in detail previously *(37)*. The convolution procedure automatically takes into account all excitation pulses necessary to describe the incomplete fluorescence relaxation of long-lived emissions such as that of Dnscho, at the repetition frequency of the source. In these cases, dark currents were also independently estimated and then fixed during the data analysis. Starting from 150 putative exponentials, plus a zero-lifetime channel taking into account light scattering of the sample, the analysis resulted, after 120 iterations, in a lifetime distribution $\alpha(\tau)$ of preexponential factors vs lifetime, which is split in as many species as peaks separated by two well-defined minima. The lifetime τ_i and relative preexponential amplitude A_i of each species i are then defined by

$$\tau_i = \frac{\int_{\text{peak } i} \tau\alpha(\tau)\, \partial\tau}{\int_{\text{peak } i} \alpha(\tau)\, \partial\tau} \tag{2}$$

and

$$A_i = \frac{\int_{\text{peak } i} \alpha(\tau)\, \partial\tau}{\int_0^\infty \alpha(\tau)\, \partial\tau} \tag{3}$$

For a mixture of noninteracting species, the preexponential amplitude A_i is proportional to the fractional population c_i of species *i* through the relationship *(34)*

$$A_i = \epsilon_i(\lambda_{exc}) k_{ri} x_i(\lambda_{em}) c_i / \sum [\epsilon_i(\lambda_{exc}) k_{ri} x_i(\lambda_{em}) c_i] \tag{4}$$

where $\epsilon_i(\lambda_{exc})$ is the molar absorption coefficient of species *i* at the excitation wavelength, k_{ri} is the radiative rate of species *i*, and $x_i(\lambda_{em})$ is the fraction at the detected wavelengths of its emission spectrum normalized to unit surface *(38)*. The first-order average fluorescence lifetime $\langle\tau\rangle$ is obtained from the lifetime distribution $\alpha(\tau)$ according to

$$\langle\tau\rangle = \frac{\int_0^\infty \tau\alpha(\tau)\, \partial\tau}{\int_0^\infty \alpha(\tau)\, \partial\tau} = \sum_i A_i\tau_i \tag{5}$$

The apparent radiative rate k_r of a fluorescent probe can be obtained from its first-order average fluorescence lifetime $\langle\tau\rangle$ and its fluorescence quantum yield Φ_f, measured under identical experimental conditions, through the relationship *(34, 39)*

$$k_r = \Phi_f/\langle\tau\rangle \tag{6}$$

The fractional contribution of species *i* to the steady-state fluorescence intensity, f_i, can be computed from its lifetime and preexponential amplitude according to

$$f_i = A_i\tau_i/\langle\tau\rangle \tag{7}$$

Error bars on the individual lifetimes τ_i are based on the average width of the corresponding peak in the lifetime distribution. Error bars on the individual amplitudes and average lifetimes $\langle\tau\rangle$ are based on the reproductibility of the measurements.

Decomposition of Fluorescence Lifetime Distributions and Average Lifetimes $\langle\tau\rangle$ in Competition Experiments. The experimental lifetime distributions $\alpha(\tau)$ in the presence of both Dnscho and a competitive antagonist at each R_{Dnscho} are expressed as weighted sums of its two characteristic lifetime distributions $\alpha_\delta(\tau)$ and $\alpha_\gamma(\tau)$ when bound to these two sites:

$$\alpha_{exp}(\tau) = f_\delta\alpha_\delta(\tau) + (1 - f_\delta)\alpha_\gamma(\tau) \tag{8}$$

where f_δ and $(1 - f_\delta)$ are the fractions of Dnscho bound respectively to the $\alpha\delta$ and $\alpha\gamma$ binding sites. Similarly, the average lifetime of bound Dnscho is expressed as

$$\langle\tau\rangle_{exp} = f_\delta\langle\tau_\delta\rangle + (1 - f_\delta)\langle\tau_\gamma\rangle \tag{9}$$

and the relative amplitude A_i for each separable component of the fluorescence lifetime distribution as

$$A_{iexp} = f_\delta A_{i\delta} + (1 - f_\delta)A_{i\gamma} \tag{10}$$

To identify these separable components and to precisely define their lifetime ranges, we employed the minima observed for the sum of all experimental distributions in a complete competition experiment for R_{Dnscho} comprised within 0.3 and 0.72. This resulted in four ranges, 0−0.7 ns, 0.7−3.1 ns, 3.1−15 ns, and 15−50 ns, within which discrete peaks could be located in all cases. The group between 3.1 and 15 ns shows variable substructures, which indicates that this group is probably heterogeneous (Figure 7). The representative lifetime of each of these groups was then

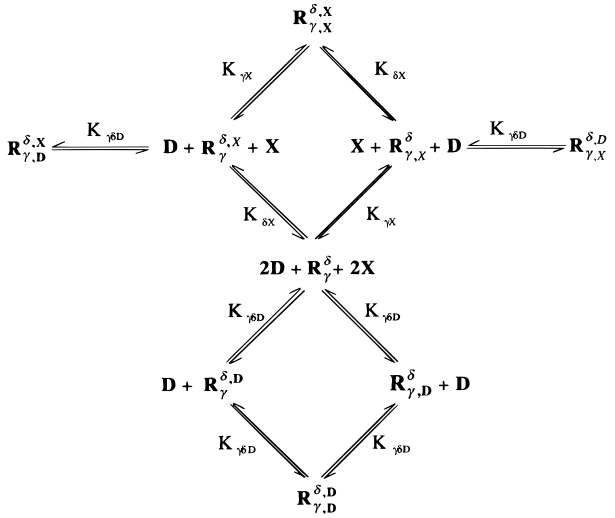

FIGURE 1: Two-site model assuming two distinct binding affinities for the competitive antagonist ($K_{\delta X}$ and $K_{\gamma X}$), a single binding affinity for Dnscho ($K_{\gamma\delta D}$), and a single allosteric state used to estimate quantitatively the different nAChR populations.

defined as the average value observed within each range. For example, in the dTC experiments (Figure 7D) the four groups display the resulting average lifetimes: 0.17 ± 0.02 ns, 2 ± 0.3 ns, 8.7 ± 0.2 ns, and 20.2 ± 0.4 ns (Table 2).

The expressions for the different fluorescence parameters are rearranged as linear functions of f_δ:

$$\alpha_{exp}(\tau) = f_\delta[\alpha_\delta(\tau) - \alpha_\gamma(\tau)] + \alpha_\gamma(\tau) \qquad (11)$$

and f_δ was first estimated at each R_{Dnscho}, by computing all required receptor populations according to the two-site model, as described below. Then the different fluorescence parameters were determined by linear regression with experimental data as the ordinate and f_δ as the abscissa, according to eqs 9 and 10. Error bars on all determined parameters are based on the standard deviation on the slope and on the abscissa axis intercept.

Expression of f_δ in Competition Experiments. The parameter f_δ is defined as the ratio of Dnscho molecules bound to the $\alpha\delta$ site over the total molecules of bound Dnscho. In competition experiments, f_δ is related to the following populations of liganded receptor:

$$f_\delta = \frac{[R_\gamma^{\delta,D}] + [R_{\gamma,D}^{\delta,D}] + [R_{\gamma,X}^{\delta,D}]}{[R_\gamma^{\delta,D}] + [R_{\gamma,D}^{\delta}] + 2[R_{\gamma,D}^{\delta,D}] + [R_{\gamma,X}^{\delta,D}] + [R_{\gamma,D}^{\delta,X}]} \qquad (12)$$

where $[R_{\gamma,X}^{\delta,D}]$ represents the concentration of the different complexes of nAChR, with the superscript corresponding to the ligand occupying the $\alpha\delta$ site and the subscript corresponding to the ligand occupying the $\alpha\gamma$ site (D = Dnscho; X = competitive antagonist).

Two-Site Model. To estimate quantitatively the different nAChR populations present during competition experiments (unliganded, monoliganded, and biliganded), we used the two-site model presented in Figure 1, which assumes that Dnscho displays an identical intrinsic affinity for the two sites ($K_{\gamma\delta D}$), whereas the competitive antagonist displays two different affinities ($K_{\delta X}$ and $K_{\gamma X}$).

This model leads to a set of 12 independent equations, from chemical equilibria, conservation of mass and experimental constraints [$R_{Dnscho} = 0.8(1 - R_X)$]. The concentration of free Dnscho [d] is expressed from this set of equations as the solution of a third degree equation, involving the binding affinities of the ligands ($K_{\gamma\delta D}$, $K_{\gamma X}$, and $K_{\delta X}$), the concentration of the free competitive ligand [x], and the total concentration of agonist binding sites. Resolution of this equation, using the method of Cardan, leads to an analytical expression for [d] as a function of $K_{\gamma\delta D}$, $K_{\gamma X}$, $K_{\delta X}$, and [x], leading to the following expression for f_δ:

$$f_\delta = \frac{[x] + m([d] + K_{\gamma\delta D})}{[x](^1/_n + 1) + 2m([d] + K_{\gamma\delta D})} \qquad (13)$$

where m and n are ratios of binding affinities defined as follows:

$$m = K_{\gamma X}/K_{\gamma\delta D} \qquad (14)$$

and

$$n = K_{\delta X}/K_{\gamma X} \qquad (15)$$

Thus, n represents the relative selectivity of the competitive ligand X toward the two binding sites. We defined p as the "competitiveness" of the competitive ligand X relative to Dnscho:

$$p = \frac{(K_{\gamma X}K_{\delta X})^{1/2}}{K_{\gamma\delta D}} \qquad (16)$$

The p value increases when the competitiveness of the ligand X decreases, whereas the n value increases with selectivity for the $\alpha\gamma$ site.

Thus, for a defined set of binding affinities, for each [x] value, a [d] will be found, and the fractions of each population and hence the fraction of Dnscho bound to the $\alpha\delta$ site (f_δ) can be deduced. The corresponding values, R_X and R_{Dnscho}, can also be calculated, since the total concentration of agonist binding sites is known. Panels A and B of Figure 2 represent, respectively, the different nAChR populations and the fraction f_δ of Dnscho bound to the $\alpha\delta$ site, as a function of the ratio of added Dnscho (R_{Dnscho}) in the case of competition experiments with dTC, modeled with binding affinities from the literature.

RESULTS

Fluorescence Properties of Dnscho. When excited at 330 nm, Dnscho in aqueous phosphate buffer displays a maximum fluorescence emission at 544 nm (Figure 3) and a very low fluorescence quantum yield (0.035), consistent with the value of 0.05 reported for Dns in water *(33)*. The fluorescence decay is nearly monoexponential, with a major lifetime of 3.3 ± 0.1 ns (Figure 4A) associated with 90% to the total amplitude, as reported previously by Herz *et al. (26)*. Our studies performed on solubilized nAChR, however, include the addition of the zwitterionic detergent CHAPS at 6.5 mM, close to the cmc *(40)*. This detergent has a significant influence on the fluorescence properties of Dnscho. Below the cmc, the fluorescence of Dnscho is slightly affected, with the major fluorescence lifetime progressively increasing from 3.3 to 3.7 ns (Table 1, Figure 4B). At the cmc, the fluorescence decay becomes multiexponential, indicating

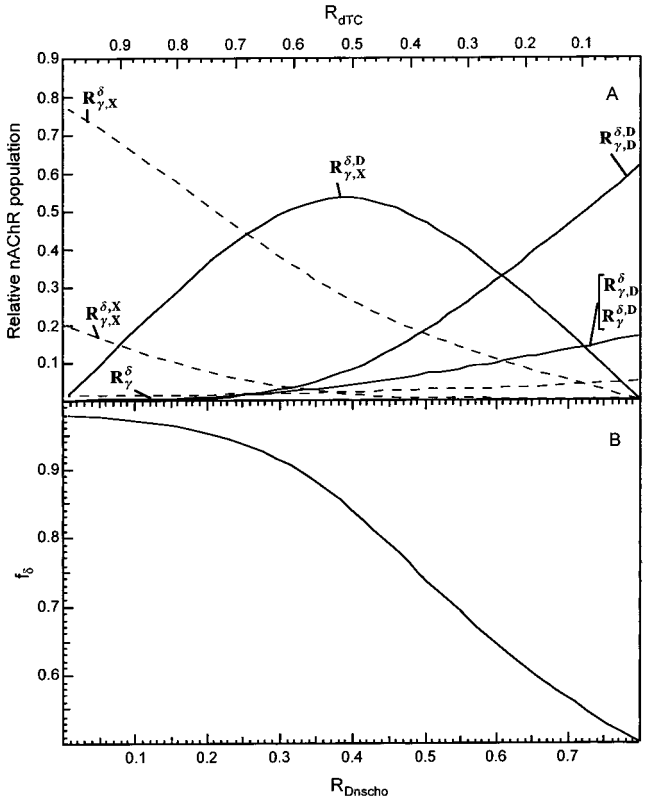

FIGURE 2: nAChR populations computed from the two-site model of Figure 1, in the presence of dTC ($K_{\delta X} = 7.7\ \mu$M, $K_{\gamma X} = 33$ nM) and Dnscho ($K_{\gamma\delta D} = 20$ nM) as described under Materials and Methods. (A) nAChR populations versus R_{Dnscho}: continuous lines represent nAChR populations carrying Dnscho, and broken lines represent nAChR populations without Dnscho. $R_{\gamma}^{\delta,X}$ and $R_{\gamma,D}^{\delta,X}$ are not represented because they are negligible. The populations were determined by solving the following equation with the Cardan method: $10[d]^3 + \{5AK_{\gamma\delta D} + 2([sites] + 4[x])\}[d]^2 + K_{\gamma\delta D}\{5BK_{\gamma\delta D} + D[sites] + 4A[x]\}[d] - K_{\gamma\delta D}^2\{4B[x] + 2A[sites]\} = 0$, where $A = (2[x](K_{\gamma X} + K_{\delta X})/K_{\gamma X}K_{\delta X} + 4$, $B = 2\{1 + ((K_{\gamma X} + K_{\delta X})[x] + [x]^2)/K_{\gamma X}K_{\delta X}\}$, and $D = ((K_{\gamma X} + K_{\delta X})[x]/K_{\gamma X}K_{\delta X}) - 6$. The parameters [x] and [d] are, respectively, the concentrations of free competitive ligand and free Dnscho, and [sites] is the concentration of total agonist binding sites, which was fixed here at 5 μM. (B) Fraction of Dnscho bound to the $\alpha\delta$ binding site versus R_{Dnscho}. Note that occupancy ratio R_{Dnscho} increases (bottom scale) when the competitive ligand ratio R_{dTC} decreases (top scale)

several microenvironments of the probe (Figure 4C). In addition to the major component centered at 3.7 ns (77%) (Figure 4B), three additional minor components are observed, and the quantum yield as well as the maximum of emission are significantly modified (Figure 3, Table 1). For CHAPS concentrations well above the CMC (62 mM), the maximum of emission is shifted to 513 nm, the quantum yield rises to 0.28 (Table 1), and the fluorescence decay is now dominated (65%) by a major long lifetime at 13.6 ns (Figures 3 and 4D).

As followed by fluorescence anisotropy decay (Figure 5), the rotational dynamics of Dnscho is strongly dependent on the presence of CHAPS micelles. At CHAPS concentrations below or equal to the cmc, the anisotropy decay is very fast, the rotational correlation time being at the limit of our time resolution, estimated to a few hundred picoseconds (Figures 5A,B). In the presence of 62 mM CHAPS, the anisotropy decay includes, in addition to the fast component, two long decay times, centered at 4 ns and 15.5 ns with respective weights of 50% and 14% (Figure 5C). The longest anisotropy

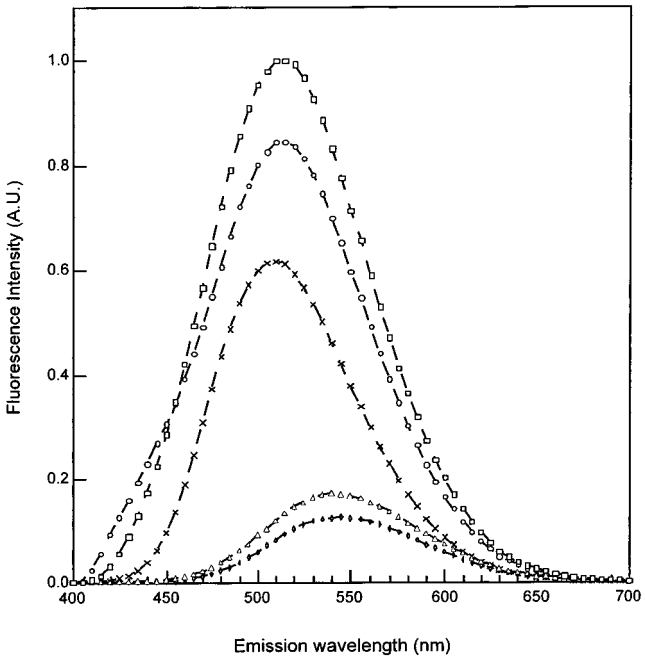

FIGURE 3: Emission fluorescence spectra of Dnscho in several environments: EtOH (×), phosphate buffer (◇), 6.5 mM CHAPS buffer (△), 62 mM CHAPS buffer (□), and bound to the nAChR at $R_{Dnscho} = 0.8$ (○). Intensities are scaled relative to the determined quantum yields. Spectra were recorded at 20 °C with an excitation wavelength of 330 nm, after subtraction of buffer fluorescence.

decay time is consistent with the rotational diffusion of a 49 Å diameter sphere, according to the Einstein−Stokes equation. This value is in good agreement with the expected dimensions of a spherical micelle formed from extended CHAPS molecules (25 Å length). These results indicate that interactions occur between Dnscho and the CHAPS micelles and possibly also with CHAPS monomers. However, at the cmc, the anisotropy decay clearly shows that the major 3.7 ns fluorescence lifetime of Dnscho is associated with a very small hydrodynamic entity, and thus plausibly with an aqueous form of the probe.

The expected proportionality relationship usually observed between the fluorescence quantum yield Φ_f and the average lifetime $\langle\tau\rangle$ for a given probe placed in various environments (EtOH, phosphate buffer, CHAPS micelles) is clearly not observed in the case of Dnscho (Table 1). The apparent radiative rates $k_r = \Phi_f/\langle\tau\rangle$ in the most apolar environments are more than 2 times higher than those observed in aqueous buffer. Li et al. *(33)* have explained this particular property of 1-substituted aminonaphthalenes by a progressive solvent-dependent change in the nature of the emissive state, changing from a ^1L_b type in apolar solvents to a ^1L_a type in polar solvents. As a result, the fluorescence lifetimes associated with Dnscho in microenvironments of highly different polarities will be differently weighted in the total fluorescence decay (eq 4). From the known dependence of preexponential factors on both the radiative rates and spectral factors, some quantitative corrections can, however, be made. For example, in the case of Dnscho in CHAPS buffer close to the cmc (Figure 4C), the peak at 3.7 ns characteristic of the free aqueous probe has an apparent amplitude 2 times lower than the peaks associated with the micellar form of the probe.

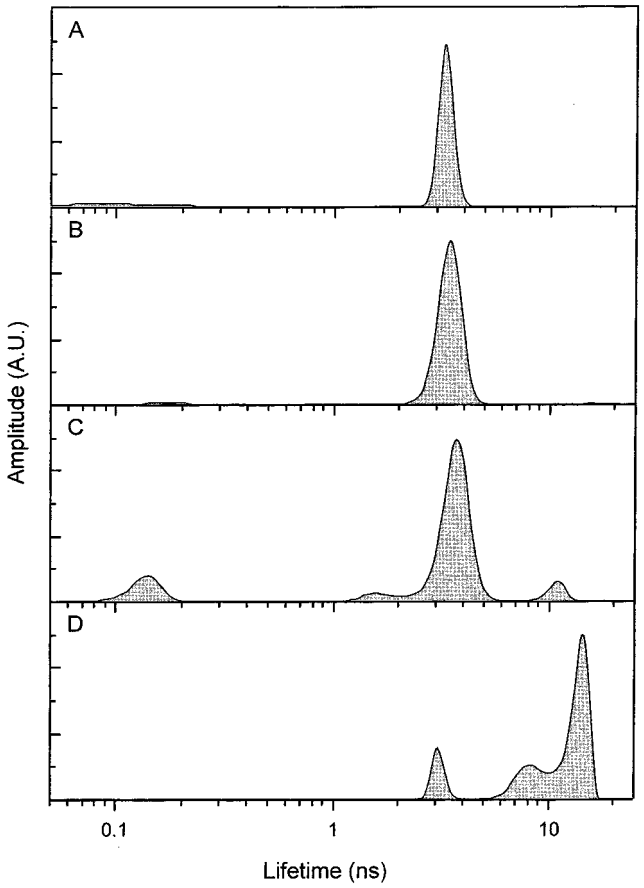

FIGURE 4: Fluorescence lifetime distributions for Dnscho in several buffers: phosphate buffer (A), 1.5 mM CHAPS buffer (B), 6.5 mM CHAPS buffer (close to the cmc value) (C), and 62 mM CHAPS buffer (D). Amplitudes are presented in arbitrary units (AU), and excitation and emission wavelengths were, respectively, 330 and 520 nm.

Table 1: Steady-State Fluorescence of Dansyl Derivatives in Different Environments[a]

probe	buffer	λ_{max} (nm)	Φ_f (%)	$\langle\tau\rangle$ (ns)	k_r ($\times 10^7$)
Dns	EtOH	510	39[b]	13.3	2.92
Dnscho	EtOH	510	17	nd	nd
Dnscho	NaP_i, 0 mM CHAPS	544	3.5	3.0 ± 0.1	1.16
Dnscho	NaP_i, 1.5 mM CHAPS	nd	nd	3.3 ± 0.1	nd
Dnscho	NaP_i, 6.5 mM CHAPS	542	4.8	3.5 ± 0.1	1.37
Dnscho	NaP_i, 62 mM CHAPS	513	28	11.0 ± 0.4	2.69
Dnscho + nAChR	NaP_i, 6.5 mM CHAPS	514	24	10.1 ± 0.5	2.37

[a] The fluorescence quantum yield Φ_f, the average lifetime $\langle\tau\rangle$ and the apparent radiative rate k_r are defined under Materials and Methods. [b] Li et al. (*33*).

Conditions Required To Observe a Specific Dnscho Signal. In the presence of nAChR, at an occupancy ratio $R_{Dnscho} = 0.8$, the fluorescence emission maximum of Dnscho is 514 nm (Figure 2), and the fluorescence quantum yield is 5 times higher than in CHAPS buffer (Table 1). The fluorescence lifetime distribution is composed of four major lifetimes: 0.2 ns (13%), 1.8 ns (14%), 7.2 ns (32%), and 18.3 ns (41%) (Table 2), with an average lifetime, defined as the summation of the components weighted for their amplitudes, of 10.1 ± 0.5 ns (Figure 6A). The characteristic lifetime of free Dnscho centered at 3.7 ns is absent (Figure 6A). For Dnscho interacting with nAChR in native membranes, Herz et al.

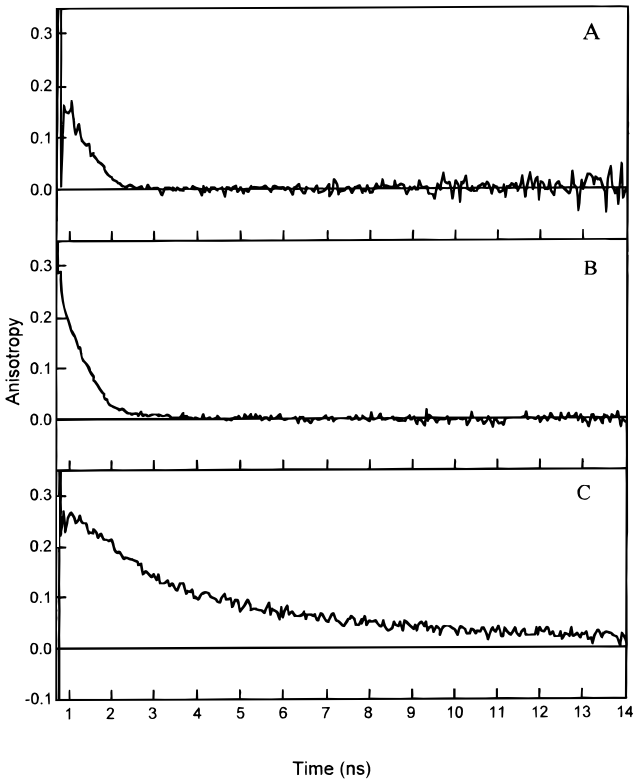

FIGURE 5: Fluorescence anisotropy decay of Dnscho in phosphate buffer (A), in 6.5 mM CHAPS buffer (B), and in 62 mM CHAPS buffer (C).

(*26*) report a biexponential decay with lifetimes at 7 and 17 ns, which correspond qualitatively to the two major components of our lifetime distributions. The lack of detection of the shortest components at 0.2 and 2 ns may be explained by the lower temporal resolution of their instrument. However, our first-order average lifetime is in good agreement with that reported by Herz et al. (9.8 ns).

At the excitation wavelength used (330 nm), the nAChR preparations give rise to a detectable autofluorescence (Figure 6B). The relative level of autofluorescence over total fluorescence varies from 2% at $R_{Dnscho} = 0.8$ to more than 40% at $R_{Dnscho} = 0.02$, whereas it is about 5% at $R_{Dnscho} = 0.3$. Indeed, when the nAChR agonist binding sites are progressively titrated by Dnscho, a strong and symmetrical increase in the average fluorescence lifetime is observed for occupancy ratios between $R_{Dnscho} = 0$ and 0.3 (Figure 6B). At low occupancy ratios, the fluorescence lifetime distributions include high weights of the two short components at 0.2 and 1.6 ns (Figure 7A). It has been impossible to reduce further this contamination, which may arise, at least in part, from the red-edge excitation and emission of the 54 tryptophan residues of the receptor itself. Therefore, in the subsequent portions of the investigations, we maintained a tight systematic control of the level of this contaminating autofluorescence, and restricted any quantitative interpretation of the data to conditions where $R_{Dnscho} \geq 0.3$, i.e., where the level of autofluorescence would not cause changes in average fluorescence lifetime higher than twice the experimental error. Also, it is clear that these short-lifetime components are likely to carry large contaminations and thus will not be interpreted in detail.

Pharmacological Specificity of Dnscho for the Agonist Binding Sites. The competitive antagonist α-Bgt is generally

Table 2: Dnscho Fluorescence Decay Parameters

		τ_1 (ns)	A_1(%)	τ_2 (ns)	A_2(%)	τ_3 (ns)	A_3(%)	τ_4 (ns)	A_4(%)	$\langle\tau\rangle$ (ns)	χ^2
					Experimental Parameters						
nAChR + Dnscho	R_{Dnscho}= 0.80	0.2 ± 0.04	13 ± 4	1.8 ± 0.1	14 ± 2	7.2 ± 0.7	32 ± 4	18.3 ± 0.6	41 ± 6	10.1 ± 0.5	1.12
nAChR + Dnscho + dTC	R_{Dnscho}= 0.32	0.18	20	1.7	9	8.2	55	20.7	16	8.1 ± 0.4	1.10
nAChR + Dnscho + α-Ctx	R_{Dnscho}= 0.32	0.17	15	1.4	16	6.5	33	17	36	8.5 ± 0.4	1.01
					Modeled Parameters						
Dnscho bound to αγ	$f_\delta = 0.0$	0.17 ± 0.02	18	2 ± 0.2	10	8.7 ± 0.5	15	20.2 ± 0.3	57	13 ± 1	
Dnscho bound to αδ	$f_\delta = 1.0$		18		14		58		10	7.2 ± 1	
nAChR + Dnscho	$f_\delta = 0.5$		18		12		36		34	10.1 ± 1	
nAChR + Dnscho + dTC	$f_\delta = 0.9$		18		14		53		15	7.7 ± 1	

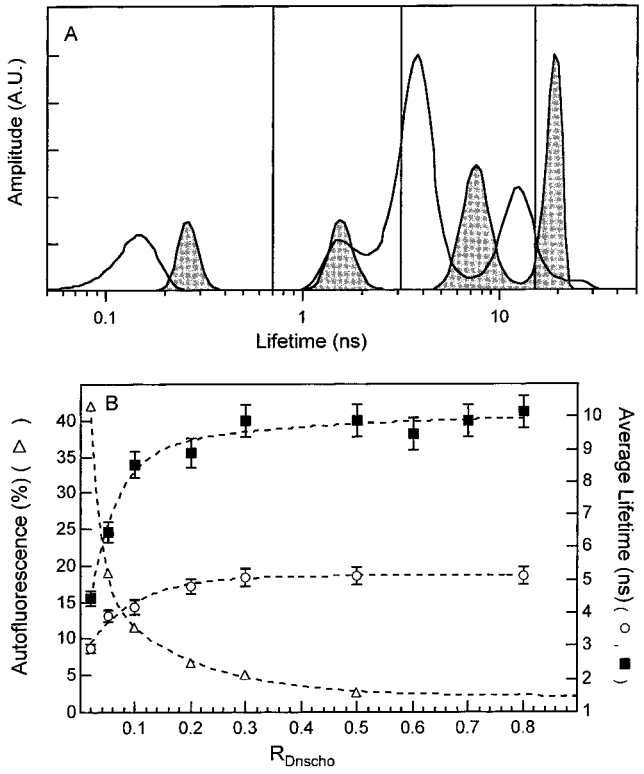

FIGURE 6: Dnscho binds specifically to the agonist binding sites. (A) Fluorescence lifetime distributions of Dnscho in the presence of nAChR (R_{Dnscho} = 0.8) with (open peaks) and without (shaded peaks) preincubation with α-Bgt. Excitation and emission wavelengths were respectively 330 and 520 nm. (B) Fluorescence average lifetimes as a function of R_{Dnscho} in the presence of nAChR with (□) and without (■) preincubation with α-Bgt, and the proportion of autofluorescence (△) versus R_{Dnscho}. The proportion of autofluorescence was estimated by comparison of the intensities of fluorescence before and after addition of Dnscho. Curves in dashed lines are for eye guidance only. The concentration of CHAPS was maintained close to the cmc (6.5 mM).

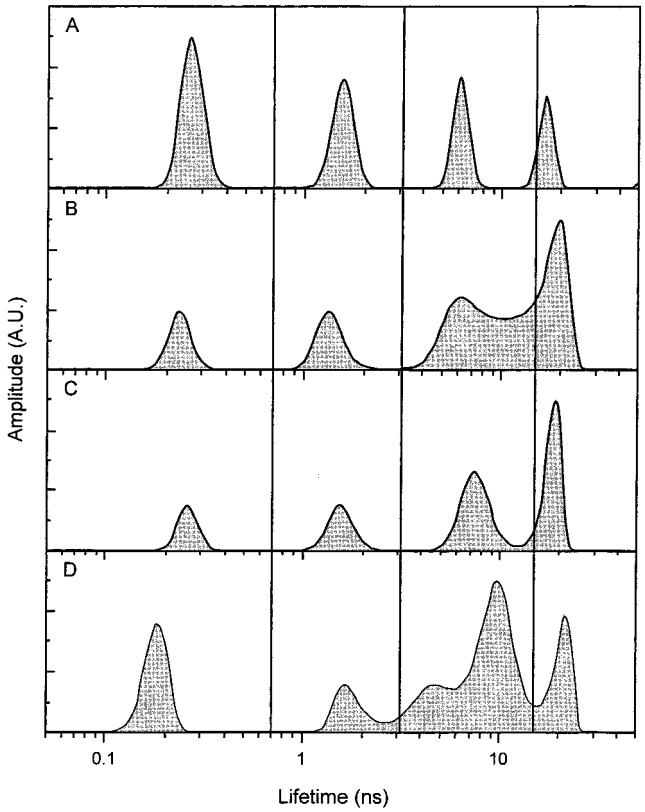

FIGURE 7: Fluorescence lifetime distributions of Dnscho bound to nAChR: without competitive ligand at R_{Dnscho} = 0.02 (A), R_{Dnscho} = 0.3 (B), and R_{Dnscho} = 0.8 (C), and with dTC R_{dTC} = 0.6 (R_{Dnscho} = 0.32) (D). The concentration of CHAPS was maintained close to the cmc (6.5 mM).

used to assess the pharmacological specificity of unknown ligands for the agonist binding sites *(26)*. After preincubation of the nAChR with a 10-fold excess of α-Bgt *(41)*, the fluorescence decay of the probe is strongly modified, producing at $R_{Dnscho} > 0.3$ an average lifetime of 5.4 ± 0.3 ns (Figure 6B), and 53% of a major component at 3.7 ns, characteristic of free Dnscho (Figure 6A). These data correspond, after corrections based on the previously determined spectra and apparent radiative rates (Table 1), to a proportion of Dnscho released into the aqueous phase of about 70%. However, three other species, centered at 0.15 ns (14%), 1.5 ns (10%), and 13.2 ns (23%), are also present in the lifetime distributions. The 13.2 ns component is consistent neither with lifetimes characteristic of Dnscho bound to the nAChR nor with free Dnscho in aqueous buffer. On the other hand, it might be consistent with some interactions between Dnscho and CHAPS micelles (Figure 4D). By contrast, at very low occupancy ratios (<0.3), the fluorescence lifetime distribution becomes progressively less sensitive to the addition of a large excess of α-Bgt (data not shown), indicating that an increasing fraction of the signal does not correspond to Dnscho bound to the agonist binding sites. Similarly, when a 10-fold excess of proadifen (a noncompetitive ligand that binds within the channel *(42)*) is added to the mixture, in either the presence or absence of α-Bgt, the fluorescence lifetime distributions are not modified (data not shown). Therefore, alternate binding of the probe to the channel of the receptor seems to be negligible in all cases.

Thus, α-Bgt is able to displace Dnscho from its primary binding sites on nAChR, as previously concluded by Heidmann and Changeux *(2)* and Herz et al. *(26)*; however, under these conditions, the displaced ligand has a complex

re-solvation pattern, where it most probably partitions between the aqueous phase and favorable locations in the CHAPS microphases. Indeed, in the presence of CHAPS-solubilized nAChR, Dnscho is in equilibrium between (i) the agonist binding sites, (ii) the CHAPS micelles, and (iii) the aqueous phase. In the absence of α-Bgt, the use of subsaturating concentrations of Dnscho (<4 μM) at agonist binding site concentrations (5 μM) well above the Dnscho K_d (20 nM) ensures that the contribution of aqueous Dnscho is negligible (at most 2%), which is also demonstrated by the absence of the characteristic lifetime. Competition experiments with α-Bgt then give an estimate of the partition equilibrium of Dnscho between the aqueous and CHAPS environments (70/30) under the same experimental conditions. From these two estimates, it can be concluded that the contribution of Dnscho bound to the CHAPS micelles should be negligible.

For R_{Dnscho} values between 0.3 and 0.8 (a range for which the autofluorescence can be neglected), the signal appears largely specific for the probe bound to the agonist binding sites. Moreover, as followed by the fluorescence lifetime distributions as well as the more stable corresponding average lifetimes, this signal is constant within the limits of experimental error (Figures 6B and 7B,C). Thus, the progressive titration of the two nonequivalent binding sites of nAChR by Dnscho gives rise to a constant, invariable signal. This shows that Dnscho remains on the average in a constant local environment along this titration experiment. This observation has two alternative and non-mutually exclusive implications: (i) Dnscho binds with a similar affinity to the two nonequivalent agonist binding sites and thus achieves an equal occupancy of both sites along the titration curve and/or (ii) the fluorescence lifetime distributions of the probe are similar in both sites, and thus any (possible) sequential binding would not be revealed through this experiment.

Pharmacological Discrimination of the Two Agonist Binding Sites by dTC and α-Ctx. To study the effects of dTC, a competitive antagonist with a higher affinity for the $\alpha\gamma$ than for the $\alpha\delta$ binding site, a fraction of the agonist binding sites was first occupied by dTC, from $R_{dTC} = 0$ to 0.7. After overnight incubation, Dnscho was added at a concentration corresponding to 80% of the free remaining sites [therefore, since $R_{Dnscho} = 0.8(1 - R_{dTC})$, the total occupancy ratio R_{Dnscho} was always greater than 0.24]. Figure 8A presents the average fluorescence lifetime of Dnscho after preincubation with increasing amounts of dTC. A progressive increase (25%) in average lifetime is observed as the concentration of the competitive ligand is reduced, i.e., when R_{Dnscho} is increased from 0.24 to 0.7. Figure 7D shows the lifetime distribution obtained for a dTC occupancy ratio of 0.6 ($R_{Dnscho} = 0.32$). In this experiment, the weight of the 20 ns component is strongly decreased, while a major peak is now observed at 9.5 ns together with a shoulder that is reminiscent of the unresolved heterogeneity sometimes observed in this region (see Materials and Methods). No peak is observed in the 3.7 ns region, showing that the observed perturbation does not result from a release of Dnscho into the aqueous phase. The fluorescence of Dnscho bound to the receptor is thus strongly modified when the agonist binding sites are partially occupied by dTC.

Similar experiments were performed with two other competitive nAChR antagonists. We first used α-Ctx, which

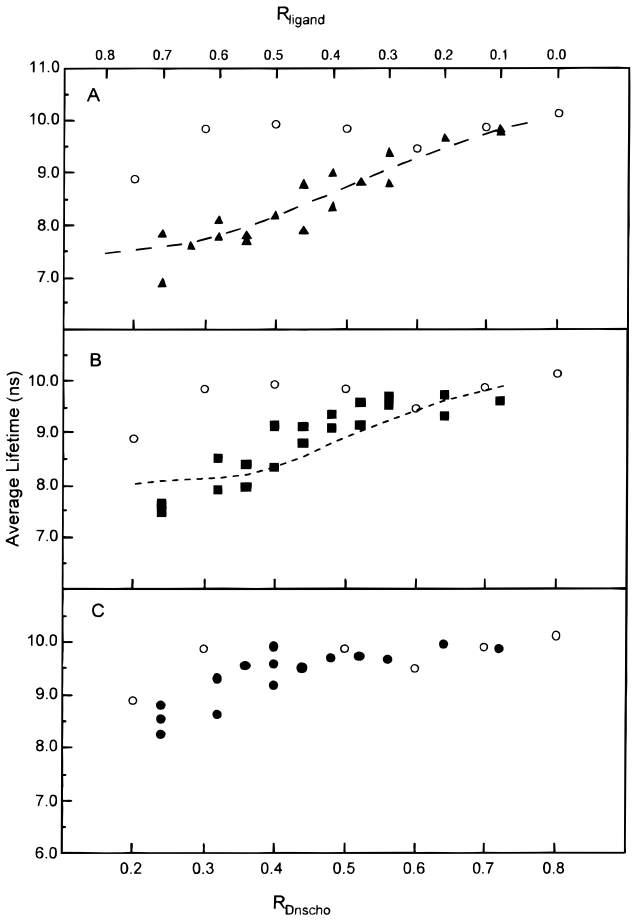

FIGURE 8: Fluorescence average lifetimes as a function of R_{Dnscho} in the presence of nAChR preincubated with different competitive antagonists. Average lifetimes obtained in the absence of competitive ligand (○) are reproduced from Figure 6B. (A) Experimental data with dTC (▲); the theoretical curve obtained according to the two-site model with dTC binding affinities from Neubig and Cohen *(16)* is shown as a dashed line. (B) Experimental data with α-Ctx (■); the theoretical curve obtained with binding affinities from Groebe et al. *(20)* is shown as a dashed line. (C) Experimental data with α-Bgt (●). The comparison of experimental data and theoretical curves was evaluated by use of the average weighted residual, defined as $\sum$ (exptl − model)^2/model. The values are, respectively, 0.19 and 0.42 for the dTC and α-Ctx curves.

was also reported to display a preferential affinity for the $\alpha\gamma$ binding site of *Torpedo californica (20)*. In the presence of increasing amounts of this ligand, the average lifetime of Dnscho bound to the remaining agonist binding sites decreases in a similar way, but the effect is slightly shifted to lower R_{Dnscho} values (Figure 8B). We also applied α-Bgt, which is expected to display a similar affinity for both sites, with a K_d in the picomolar range *(21)*. In this experiment, the average lifetime of Dnscho increases weakly but significantly from $R_{Dnscho} = 0.2$ to 0.4 and then remains constant for R_{Dnscho} beyond 0.4 (Figure 8C). Therefore, the signal of bound Dnscho appears much less sensitive to the partial occupancy of the other agonist binding site by α-Bgt, than by dTC and α-Ctx.

Thus, competition with α-Ctx and dTC, which are chemically unrelated but display a preferential affinity for the same site, results in comparable effects on Dnscho fluorescence, with a decrease in average fluorescence lifetime. In the simplest interpretation of these results, it can be assumed that the fluorescence lifetime distribution of Dnscho is

different at the two sites, with a shorter average lifetime for the αδ site. Competition with the selective ligands α-Ctx and dTC would then simply increase the relative proportion of the αδ site in the total fluorescent signal in both cases. More complex interpretations, involving site−site perturbations depending on the ligands bound, do not seem to be required at this stage. If this simple description of two noninteracting binding sites is correct, the observed fluorescence lifetime distributions at each point of a competition experiment is a linear combination of two characteristic lifetime distributions, $\alpha_\delta(\tau)$ and $\alpha_\gamma(\tau)$ (eq 8). In addition, since the fluorescence lifetime distributions of Dnscho in the absence of competing ligands do not show significant changes in the range $R_{\mathrm{Dnscho}} = 0.3-0.8$ (Figure 6B,C), these two sites must have been titrated in a parallel and equivalent manner, and therefore Dnscho displays a nearly equivalent affinity for these two sites [alternative hypothesis (i) above].

Decomposition of the Respective Dnscho Fluorescence Decay Parameters of Dnscho Bound to the Two Agonist Binding Sites. We have derived a two-site model to describe our competition experiments with dTC (Figure 1). This model assumes a single conformation of the nAChR (see Discussion) and a competitive ligand with two possibly distinct affinities. By use of published values of the different K_ds *(16, 20)*, this model provides a quantitative prediction of the relative fraction of Dnscho bound to each site for any given value of R_{dTC}. These computations show that when $R_{\mathrm{dTC}} = 0.6$, 90% of the binding sites occupied by Dnscho are αδ sites (f_δ) (Figure 2B). Therefore, the high selectivity and affinity of dTC allows the direct observation of the nearly pure fluorescence lifetime distribution of Dnscho bound to the αδ site. On the basis of this model, we have used the dTC data to delineate through a least-squares fit (Materials and Methods) the characteristic average lifetimes of Dnscho bound to each site. This results in the respective values 7.2 ± 1 ns for αδ and 13 ± 1 ns for αγ, confirming that the fluorescence properties of Dnscho are strongly different in each site. Strikingly, this simple model fits satisfactorily the data set of Figure 8A.

We used a similar approach to evaluate the respective amplitudes of individual components in the fluorescence lifetime distributions, when Dnscho is bound to either the αδ or αγ binding sites. The resulting reconstructed lifetime distributions (Figure 9 and Table 2) suggest that Dnscho still has a multiexponential fluorescence decay in both sites. Dnscho bound to the αδ site has a low contribution to the 20.2 ns lifetime (10%) and a major component at 8.7 ns (58%). Conversely, Dnscho bound to the αγ site has a major component at 20.2 ns (57%) and a low contribution to the 8 ns region (15%). The identical contribution of both sites to the two short lifetimes at 0.2 and 2 ns may actually reflect the lack of specificity of these components, which may arise from autofluorescence of the nAChR samples and/or residual nonspecific binding of Dnscho. The reconstitutions of various decay parameters from these model distributions, including average fluorescence lifetimes, are in good agreement with the corresponding experimental data (Table 2).

We also examined the consistency of the α-Ctx experiments with these results. We again used the same two-site model, together with α-Ctx affinity constants from the literature *(20)*. Although these values pertain to different *Torpedo* species, the average lifetimes obtained for Dnscho

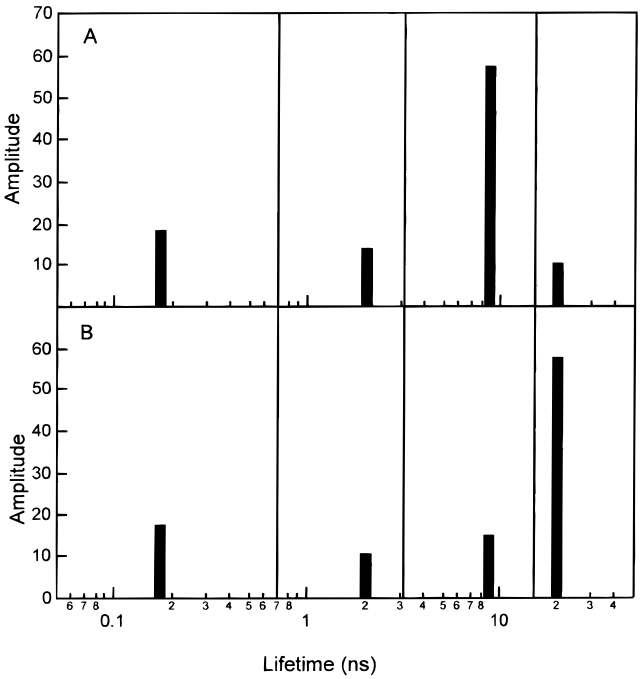

FIGURE 9: Computed fluorescence lifetime distributions of Dnscho. The lifetime ranges are delineated by vertical lines. (A) Dnscho bound to the αδ agonist binding site. (B) Dnscho bound to αγ agonist binding site. These theoretical lifetime distributions were determined from modeling of experiments with dTC, with binding constants from the literature.

bound to the αδ and αγ sites are respectively 8 ± 1.4 ns and 12 ± 1.4 ns, i.e., in reasonable agreement with those extracted from dTC experiments. However, the fit of the α-Ctx data to this simple model (Figure 8B) is somewhat less satisfactory than of the dTC data (Figure 8A).

Sensitivity of Dnscho Average Fluorescence Lifetimes to the Selectivity of Competitive Ligands. A given ligand may be characterized by two independent quantities: first, its relative selectivity, $n = K_{\delta X}/K_{\gamma X}$, for one of the two agonist binding sites, and second, its average binding affinity *relative to Dnscho*, $p = (K_{\delta X}K_{\gamma X})^{1/2}/K_{\delta\gamma D}$, which we will term here its competitiveness. The sensitivity of our method will depend on both these parameters (eqs 13−16). The selective binding of the ligand will be manifested by a change $\Delta\tau$ in the apparent average lifetime of Dnscho in the presence of the ligand. On the basis of our estimates of average fluorescence lifetime accuracy (5%), this change will be measured with confidence, if it exceeds 1 ns in the range of R_{Dnscho} between 0.32 and 0.72.

We performed simulations to evaluate the average lifetime changes $\Delta\tau$ expected for different (n, p) couples in the case of ligands analogous to dTC (Figure 10A). From these computations, it can be noted that very small differences in relative binding affinities (n value) can be detected (see the 1 ns curve in Figure 10A), if a sufficiently competitive ligand is used. Second, a given difference $\Delta\tau$ can correspond either to a limited p range and a large range of n values or to a well-defined n value and a large range of p values. These two alternatives correspond to two different domains for the relative competitiveness p of the ligand (either poorly or highly competitive). However, all curves of $\langle\tau\rangle$ vs R_{Dnscho} corresponding to the same $\Delta\tau$ but to very different couples (n, p) are nearly identical (Figure 10B). Thus, the shape of

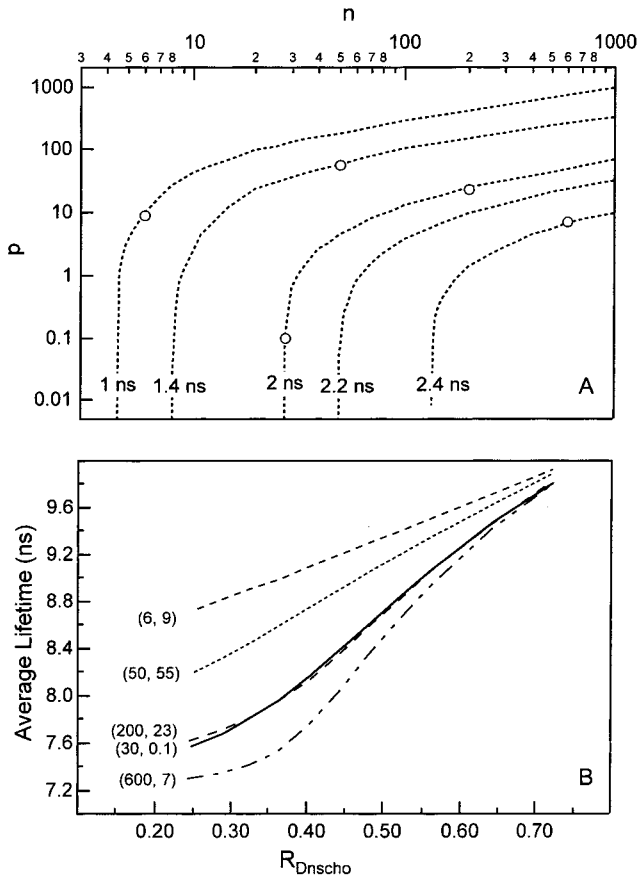

FIGURE 10: Pharmacological sensitivity of the Dnscho time-resolved fluorescence signal. (A) (n, p) values corresponding to average lifetime differences $\Delta\tau$ of 1, 1.4, 2, 2.2, and 2.4 ns, where $n = K_{\delta X}/K_{\gamma X}$ and $p = (K_{\delta X}K_{\gamma X})^{1/2}/K_{\gamma\delta D}$. The average lifetime difference is calculated from the values at $R_{Dnscho} = 0.32$ and $R_{Dnscho} = 0.72$. The concentration of agonist binding sites is 5 μM. (B) Simulations of fluorescence average lifetime evolutions for Dnscho in the presence of nAChR preincubated with a competitive ligand, for various (n, p) values also indicated in the top figure (○), where (n, p) are (6, 9), (50, 55), (200, 23), (30, 0.1), and (600, 7). Note that (200, 23) and (30, 0.1) correspond to the same lifetime difference $\Delta\tau$ in the top figure and are not distinguishable.

these curves cannot be used to discriminate between these two alternatives. Instead, one of these can be selected, if for example the order of magnitude of p is known, according to binding experiments.

From the mean affinity of the competitive ligand $(K_{\delta X}K_{\gamma X})^{1/2}$, as obtained from classical binding experiments, the value of p is determined. This, together with the $\Delta\tau$ value observed, will correspond to a value of n. For example, in the case of the high-affinity ligand α-Bgt ($K_d = 20$ pM, $p = 0.001$), the value of $\Delta\tau = 0.8$ ns is inferior to the limit of detection (1 ns). Hence, it can be concluded that the selectivity ratio for $\alpha\gamma$ versus $\alpha\delta$ cannot exceed $n = 5$. In the case of dTC, which displays a weak competitiveness ($p = 25.2$), the large variation $\Delta\tau$ close to 2 ns shows that the affinity difference must be at least 200-fold. However, cases relatively undetermined can occur, such as that of α-Ctx. In this case, the $\Delta\tau$ value (1.4 ns) reflects either a strong affinity $p < 10$ $[(K_{\delta X}K_{\gamma X})^{1/2} < 200$ nM] and a moderate selectivity close to 10, or a low intrinsic affinity $p > 10$ and a stronger selectivity $n > 10$. Neither of these alternate possibilities is in agreement with the data from literature ($K_{\gamma X} = 2.6$ nM, $K_{\delta X} = 2.3$ μM, $n = 883$, and $p = 3.87$), which might explain the unsatisfactory fit of our data with these values (Figure 8B). This problem could also reflect the known species dependency of the apparent affinities of α-Ctx binding to nAChRs *(18)*, or alternatively an inadequacy of the simple two-site model when extrapolated from dTC to α-Ctx (see Discussion).

DISCUSSION

In the experiments reported here, the time-resolved fluorescence signal of Dnscho was employed to investigate the microenvironment of the nicotinic agonist when bound to each of the two nicotinic binding sites of the *Torpedo marmorata* nAChR. The strong sensitivity of this signal to a large excess of α-Bgt, together with its insensitivity to proadifen, shows that, under the experimental conditions used, it reflects the specific binding of Dnscho to the nicotinic binding sites. This characteristic signal is heterogeneous: it is composed of four separable exponential components, with the two major components qualitatively consistent with those reported from previous studies performed on native nAChR-rich membranes *(26)*. The fluorescence of Dnscho bound to the CHAPS-solubilized nAChR is thus similar to that of Dnscho bound to the protein in native membranes, indicating that our artificial solubilization conditions maintain the integrity of the agonist binding sites.

We found that the fluorescence decay remains constant irrespective of the Dnscho binding ratio in the absence of other competitive ligands. However, the fluorescence decay dramatically changes when either of two chemically unrelated competitive antagonists, dTC and α-Ctx, is progressively added. Both ligands are known to display a binding preference for the $\alpha\gamma$ site of the *Torpedo* receptor. The observed variations of the fluorescence lifetime distributions as a function of the dTC concentration are readily interpreted with the simple assumption that the receptor possesses two sites with different structures and pharmacologies and that Dnscho displays different fluorescence signatures when bound to each of these sites. Furthermore, directly applying the equilibrium binding constants of Dnscho and dTC from previously published determinations leads to an adequate description of the data, permitting, in a first approximation, a simple additive description of the signal.

According to the reconstructions obtained from this two-site model, Dnscho in the $\alpha\delta$ site has a major lifetime at 8.7 ns, whereas in the $\alpha\gamma$ site, it has a major lifetime at 20.2 ns. Therefore, as originally suggested by Herz et al. *(26)*, the observed heterogeneity of Dnscho fluorescence on the *Torpedo* nAChR arises principally from the structural heterogeneity of the agonist binding sites. Nevertheless, each binding site displays a characteristic heterogeneous fluorescence decay. It is, however, difficult to assess, at the present stage, whether this heterogeneity arises from uncertainties on the data, from contributions of nonspecific fluorescence, or from definite physical or chemical exchanges at each of the agonist binding sites.

An interesting conclusion of our study is that although Dnscho lies in different microenvironments in each of its two agonist binding sites, the relative binding affinity for each of the two sites is equivalent. This finding shows that the high affinity of the probe for the receptor is governed mainly by specific interactions with the choline moiety of the molecule, leading to a nearly unperturbed affinity [$K_d =$

20 nM *(2)*] compared to the natural neurotransmitter [K_d = 14 nM *(16)*]. The dansyl chromophore may actually be quite distant from the choline group pharmacophore, if the Dnscho molecule binds in an extended conformation (around 24 Å). Still, the maximum of fluorescence emission of the dansyl group bound to the nAChR indicates an average environment nearly equivalent to ethanol, showing that it is located in a hydrophobic pocket inside the protein. Our results are also in good agreement with photolabeling studies, showing that competitive ligands have distinct microenvironments, depending on the nature of the complementary subunit (γ or δ) *(8, 43)*. Additional evidence, including anisotropy decay, collisional quenching, and spectral studies, show that dansyl has markedly different microenvironments and dynamics in its two nonequivalent binding sites (manuscript in preparation).

Strongly nonidentical affinities of ligands for the two nAChR sites have been investigated by the binding of radioactive ligands and photolabeling studies, combined with mutagenesis *(8, 11, 15, 44)*. Following the change in average fluorescence lifetime of Dnscho during competition experiments with unknown ligands now appears as a sensitive method to qualitatively assess site selectivity and further to identify the site preferentially bound. A decrease in $\langle\tau\rangle$ in the presence of the competitive ligand will indicate its preference for the $\alpha\gamma$ site, while an increase in $\langle\tau\rangle$ will indicate a preference for the $\alpha\delta$ site. As shown by the simulations in Figure 10, the degree of quantitative information that can be obtained will depend on the relative competitiveness of the ligand compared to Dnscho. If the ligand is strongly displaced by Dnscho ($p > 10$), selectivity will be detectable, and it will be possible to give an order of magnitude for the selectivity ratio n. If the ligand is highly competitive, a relatively accurate value of n can be specified.

Our model involves a single molecular form of the receptor, although a large body of experimental data, including equilibrium binding as well as rapid mixing and ion flux experiments *(2)*, indicates that the receptor spontaneously undergoes transitions between four states, characterized by different intrinsic binding affinities and channel gating: a basal B, an active A, and two desensitized I and D states. It is, however, likely that the state observed in dTC experiments corresponds to the D state: indeed, both Dnscho and dTC are known to shift the allosteric transitions in favor of the D state at equilibrium *(2, 17)*. This conclusion is also supported by the fact that the fluorescence decay of Dnscho is unaffected by the binding of the desensitizing noncompetitive blocker proadifen *(45)*. The reported fluorescence lifetime distributions in dTC experiments thus most probably reflect the Dnscho microenvironment in the desensitized conformational state of nAChR. However, in the case of ligands strongly stabilizing the basal state B, the microenvironment of Dnscho could be modified. Photolabeling studies with DDF have shown that substantial structural changes take place between these two conformations *(17)*. Therefore, the information provided by our method are fully reliable only in the case of ligands that stabilize the same receptor conformational state as Dnscho.

Within these restrictions, the Dnscho time-resolved fluorescence method constitutes an interesting and straightforward approach to establish the site selectivity of unknown ligands of neuromuscular types of nAChR that is complementary to conventional radioactive binding experiments. This method may be effectively applicable to a large family of nAChR ligands, as long as their dissociation constant for the agonist sites is smaller than 10 μM, and they belong to the category of desensitizing ligands. Systematic studies with ligands known to stabilize the resting state B could aid in achieving a better understanding of the interplay between conformational transitions and site heterogeneity in the fluorescence properties of Dnscho, and thus to expand further the scope of our method. Also, in the light of information obtained on muscle-type receptors such as *T. marmorata*, it would be now of interest to dissect the modes of interaction of Dnscho with neuronal or homo- or heterooligomeric types of receptors, as well as with mutants showing various perturbations of their allosteric responses.

ACKNOWLEDGMENT

We thank the LURE technical staff for operating the synchrotron machine, J. L. Eiselé for technical instruction, A. Devillers-Thierry for critical reading of the manuscript, and J. M. Betton for providing access to his steady-state spectrofluorometer.

REFERENCES

1. Edelstein, S. J., and Changeux, J. P. (1998) *Adv. Protein Chem. 51*, 121−184.
2. Heidmann, T., and Changeux, J. P. (1979) *Eur. J. Biochem. 94*, 255−279.
3. Blount, P., and Merlie, J. P. (1989) *Neuron 3*, 349−357.
4. Oswald, R. E., and Changeux, J. P. (1982) *FEBS Lett. 139*, 225−229.
5. Kao, P. N., Dwork, A. J., Kaldany, R. R., Silver, M. L., Wideman, J., Stein, S., and Karlin, A. (1984) *J. Biol. Chem. 259*, 11662−11665.
6. Langenbuch-Cachat, J., Bon, C., Mulle, C., Goeldner, M., Hirth, C., and Changeux, J. P. (1988) *Biochemistry 27*, 2337−2345.
7. Abramson, S. N., Li, Y., Culver, P., and Taylor, P. (1989) *J. Biol. Chem. 264*, 12666−12672.
8. Pedersen, S. E., and Cohen, J. B. (1990) *Proc. Natl. Acad. Sci. U.S.A. 87*, 2785−2789.
9. Chiara, D. C., and Cohen, J. B. (1997) *J. Biol. Chem. 272*, 32940−32950.
10. Corringer, P. J., Le Novère, N., and Changeux, J. P. (2000) *Annu. Rev. Pharmacol. Toxicol. 40*, 431−458.
11. Sine, S. M. (1993) *Proc. Natl. Acad. Sci. U.S.A. 90*, 9436−9440.
12. Corringer, P. J., Galzi, J. L., Eisele, J. L., Bertrand, S., Changeux, J. P., and Bertrand, D. (1995) *J. Biol. Chem. 270*, 11749−11752.
13. Martin, M., Czajkowski, C., and Karlin, A. (1996) *J. Biol. Chem. 271*, 13497−13503.
14. Sine, S. M., Kreienkamp, H., Bren, N., Maeda, R., and Taylor, P. (1995) *Neuron 15*, 205−211.
15. Pedersen, S. E., and Papineni, R. V. L. (1995) *J. Biol. Chem. 270*, 31141−31150.
16. Neubig, R. R., and Cohen, J. B. (1979) *Biochemistry 18*, 5464−5475.
17. Galzi, J. L., Revah, F., Bouet, F., Menez, A., Goeldner, M., Hirth, C., and Changeux, J. P. (1991) *Proc. Natl. Acad. Sci. U.S.A. 88*, 5051−5055.
18. Hann, R. M., Pagan, O. R., and Eterovic, V. A. (1994) *Biochemistry 33*, 14058−14063.
19. Kreienkamp, H. J., Sine, S. M., Maeda, R. K., and Taylor, P. (1994) *J. Biol. Chem. 269*, 8108−8114.
20. Groebe, D. R., Dumm, J. M., Levitan, E. S., and Abramson, S. N. (1995) *Mol. Pharmacol. 48*, 105−111.
21. Weber, M., and Changeux, J. P. (1974) *Mol. Pharmacol. 10*, 1−14.

22. Edelstein, S. J., Schaad, O., and Changeux, J. P. (1997) *Biochemistry 36*, 13755−13760.
23. Edelstein, S. J., Schaad, O., and Changeux, J. P. (1997) *C. R. Acad. Sci., Ser. 3 320*, 953−961.
24. Jackson, M. B., Konnerth, A., and Augustine, G. J. (1991) *Proc. Natl. Acad. Sci. U.S.A. 88*, 380−384.
25. Johnson, D. A., Voet, J. G., and Taylor, P. (1984) *J. Biol. Chem. 259*, 5717−5725.
26. Herz, J. M., Johnson, D. A., and Taylor, P. (1989) *J. Biol. Chem. 264*, 12439−12448.
27. Valenzuela, C. F., Weign, P., Yguerabide, J., and Johnson, D. A. (1994) *Biophys. J. 66*, 674−682.
28. Arias, H. R. (1997) *Brain Res. Brain Rev. 25*, 133−191.
29. Prinz, H., and Maelicke, A. (1992) *Biochemistry 31*, 6728−6738.
30. Waksman, G., Changeux, J. P., and Roques, B. P. (1980) *Mol. Pharmacol. 18*, 20−27.
31. Saitoh, T., and Changeux, J. P. (1980) *Eur. J. Biochem. 105*, 51−62.
32. Sobel, A., Heidmann, T., Cartaud, J., and Changeux, J. P. (1980) *Eur. J. Biochem. 110*, 13−33.
33. Li, Y. H., Chan, L. M., Tyer, L., Moody, R. T., Himel, C. M., and Hercules, D. M. (1975) *J. Am. Chem. Soc.*, 3118−3126.
34. Wahl, P. (1975) in *New techniques in biophysics and cell biology* (Pain, H., and Smith, B., Eds.) pp 233−285, Wiley, London.
35. O'Connor, D. V., and Phillips, D. (1984) *Time correlated single photon counting*, Academic Press, London.
36. Deville-Bonne, D., Sellam, O., Mérola, F., Lascu, I., Desmadril, M., and Veron, M. (1996) *Biochemistry 35*, 14643−14650.
37. Blandin, P., Mérola, F., Brochon, J. C., Tremeau, O., and Menez, A. (1994) *Biochemistry 33*, 2610−2619.
38. Birks, J. B. (1970) *Photophysics of aromatic molecules*, John Wiley & Sons Ltd., London.
39. Mérola, F., Rigler, R., Holmgren, A., and Brochon, J. C. (1989) *Biochemistry 28*, 3383−3398.
40. Schurholz, T., Kehne, J., Gieselmann, A., and Neumann, E. (1992) *Biochemistry 31*, 5067−5077.
41. Changeux, J. P., Kasai, M., and Lee, C. Y. (1970) *Proc. Natl. Acad. Sci. U.S.A. 67*, 1241−1247.
42. Pedersen, S. E., Sharp, S. D., Liu, W. S., and Cohen, J. B. (1992) *J. Biol. Chem. 267*, 10489−10499.
43. Dennis, M., Giraudat, J., Kotzyba-Hibert, F., Goeldner, M., Hirth, C., Chang, J. Y., Lazure, C., Chretien, M., and Changeux, J. P. (1988) *Biochemistry 27*, 2346−2357.
44. Sine, S. M., Quiram, P., Papanikolaou, F., Kreienkamp, H. J., and Taylor, P. (1994) *J. Biol. Chem. 269*, 8808−8816.
45. Heidmann, T., Oswald, R. E., and Changeux, J. P. (1983) *Biochemistry 22*, 3112−3127.

BI992811P